13th IEA Heat Pump Conference
April 26-29, 2021 Jeju, Korea

Dynamic modeling and charge minimization study of a packaged propane heat pump with external flow reversal for cold climates

Tyler J. SHELLY[a] , Riley B. BARTA[a] , Davide ZIVIANI[a,*], Eckhard A. GROLL[a]

[a]Ray W. Herrick Laboratories, School of Mechanical Engineering, Purdue University
West Lafayette, 47907-2099, USA
tshelly@purdue.edu; bartar@purdue.edu; dziviani@purdue.edu; groll@purdue.edu

Abstract

Buildings consume approximately 40% of the primary energy used in the U.S. The energy-independence challenge is particularly acute for buildings in colder U.S. climates that have a longer heating season. Heating is by far the biggest consumer of energy, accounting for at least 30%, and in some cases as much as 60%, of total energy use. In addition, the gradually phase-down of current refrigerants requires further research to identify suitable low-global warming potential (GWP) replacements. Hydrocarbons represent a possible solution, but their flammability yields to a number of challenges towards the actual commercialization in the residential sector. In this paper, a packaged air-source heat pump with external flow reversible is proposed as a viable solution to safely utilizing flammable refrigerants, such as propane (R-290). The proposed system can also be adapted to serve as a cold-climate heat pump that provides heating, cooling, and domestic hot water. A detailed dynamic model has been developed to evaluate the performance benefits of the proposed system architecture. Moreover, the use of propane as the working fluid reduces the total charge required by the system, which yields to possible down-sizing of the equipment. To this end, a charge minimization study has been carried out to further investigate the trade-off between reduced charge inventory and performance.

© HPC2020.
Selection and/or peer-review under responsibility of the organizers of the 13th IEA Heat Pump Conference 2020.

Keywords: Cold-Climate Heat Pump, Seasonal Modeling, Propane, Charge Sensitivity

1. Introduction

As the adverse environmental effects of using hydrofluoricarbon (HFC) refrigerants become more and more apparent, the efforts towards developing technology to efficiently utilize alternative refrigerants has grown significantly. Specifically, R-290 (propane) is being considered due to its negligible global warming potential (GWP) and ozone depletion potential (ODP). However, propane inside a residential heat pump needs to be combined with a secondary loop due to its flammability. Commonly, R-290 heat pumps are paired with Ethylene Glycol/water (EG) secondary loops that can travel through the home. Application of this technology in northern regions of the US presents several challenges, with the largest being the broad range of both heating and cooling ranges necessary in this region. The components selected need to strike a balance between efficiency and being able to meet requirements over large operating conditions. According to a 2014 Northeast/Mid-Atlantic Air-Source Heat Pump Marketing Strategies Report [1], the adoption of air-source heat pumps in homes that currently use electricity, oil, or Propane furnaces for heating in the Northeast/Mid-Atlantic region could result in an annual savings of $1.2 Billion and over 7 million metric tons of annual carbon emissions. Additionally, the report found that the average heat pump capacity in the Massachusets market is 2.3 tons. According to the Department of Energy [2], the minimum required seasonal performance for these

* Corresponding author. Tel.: +1-619-496-9011.
E-mail address: dziviani@purdue.edu.

heat pumps is an 8.2 heating seasonal performance factor (HSPF) and a 14 seasonal energy efficiency ratio (SEER).

Wang et al. [3] performed a comprehensive literature review on the advantages of using hydrocarbon refrigerants in secondary loop heat pumping systems. In addition to increased safety, lower charge levels, and potentially reduced operating costs, it was found that hydrocarbons saw an average of 9.6% improvement in performance over fluoronated refrigerants while in heat pumping applications. Palm [4] concluded that the Coefficient of Performance (COP) of systems using hydrocarbon refrigerants would be equal to or greater than those of systems using R-134a or R-22, and also found that the majority of components for HFC systems can be used in R-290 sytems. Some disadvantages listed by this paper are the smaller number of compressors available in high-capacity ranges, as well as the danger of flammability. Park and Jung [5] experimentally compared R-290 and other hydrocarbons in air conditioning application and found that R-290 achieved a 1.9% higher COP but had 11.5% smaller cooling capacity. However, the paper found that this result was achieved with less than 50% mass of charge. Fernando et al. [6] experimentally validated the temperature profile through an evaporator that legitimizes the decision to use glycol as a seondary loop fluid, as shown in Fig. 1. Additionally, Fernando found that small propane charges in heat pump applications both increase the safety of the system, and also still result in similar COP to HFC systems under similar operating conditions.

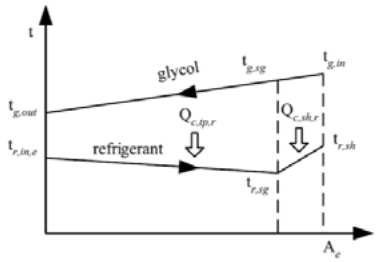

Fig. 1. Evaporator temperature profile [6].

A 50/50 combination of EG will reduce the freezing temperature of the secondary loop fluid to below -33℃, making it safe for use during the coldest temperatures measured in the Boston area, and is non-toxic. Ginies et al. [7] studied the effects of low-solubility oils in R-290 refrigeration systems in an effort to allow end users to utilize larger capacity units while staying within safety standards set by EN378, ISO5149, and the like. The study focused on Polyalkylene Glycol (PAG) and Polyolester (POE) oils, and found that when the correct oil is chosen for a 0.1 kg R-290/kW in a 60 kW system, the charge could be reduced by 18-30% without compromising capacity.

While many technologies aimed at increasing vapor compression cycle (VCC) have been investigated, there is often difficulty justifying increased completixty to obtain performance benefits. As such, generally only solutions that are both simple and efficient are widely accepted. One of these methods is known as economization, which comes in two forms. First, a flash tank can be placed in the expansion process to separate phases in a two-phase flow, allowing saturated liquid to enter the evaporator and bypassing the vapor to the compressor. This strategy has been proven to be controllable without compromising compressor suction superheat by Xu et al. [8]. The second form of economization is known as closed economization and achieved with an internal heat exchanger (IHX), which can be effectively controlled with an electronic expansion valve (EXV) [9]. Economization also allows vapor injection into the compressor at specific points, with increased precision on the superheat control. In theory, an infinite number of injection ports can be used to achieve saturated-vapor compession and can result in up to 51% COP improvement in an R-404A cycle. However, 75% of this performance benefit can be achieved with only three injection ports, which is considered to be the practical limit by Mathison et al. [10].

Multi-stage compression technology applied in a cold climate heat pump (CCHP) has been investigated via simulation by Caskey [11]. In this work, a gas heating system was compared to a two-stage heat pump in US Army barracks located in the central and northern US. The analysis resulted in a predicted CO_2 reduction by 33.5% while simultaneously reducing the heating cost by 25%. Gschwend et al. [12] further analyzed

possibilities to reduce power consumption of barrack buildings for the U.S. Army. The researchers concluded that the use of a two-stage heat pump lead to a seasonal COP of approximately 3.0, along with potential energy savings of 20% – 35% in the existing buildings.

This work presents the design and modeling of a packaged vapor-injected (VI) two-stage R-290 VCC featuring two EG/Water secondary loops and external flow reversal for hydronic heating and cooling of a residential home. The design focuses on cold climates, thus designating this work a CCHP. A 5-ton system design is proposed, annual data is analyzed for Boston, USA, and the system is assessed for performance in both weather datasets at two design temperatures. A dynamic and detailed model of the system has been developed and utilized to assess the impact of charge inventory.

2. System Design and Approach

2.1. System overview

The proposed R-290 – EG heat pump schematic is shown in Fig. 2. The VCC uses 2-stage compression with VI in the intermediate stage. An IHX is utilized to facilitate closed economization with the dual purpose of further sub-cooling the flow from the condenser outlet and superheating the economized vapor to be injected into the compressor. All three system heat exchangers will be plate heat exchangers (PHX). The IHX used for economization will be the smaller capacity heat exchanger (HX), while the condenser and evaporator will be larger PHXs that transfer heat between R-290 and the EG secondary loop. There is no 4-way valve associated with the VCC because the EG loop enters a multi-input multi-output (MIMO) valve which enables transition between heating and cooling modes to the home. Additional components in the VCC include an oil separator located at the second stage discharge that returns the oil to the suction of the first stage of compression, as well as a suction-line accumulator to ensure no 2-phase flow enters the compressor suction port. A filter-drier is located at the outlet of the condenser to remove potential contaminants from the R-290, and there is also a liquid receiver placed at the inlet to the sub-cooler for charge modulation.

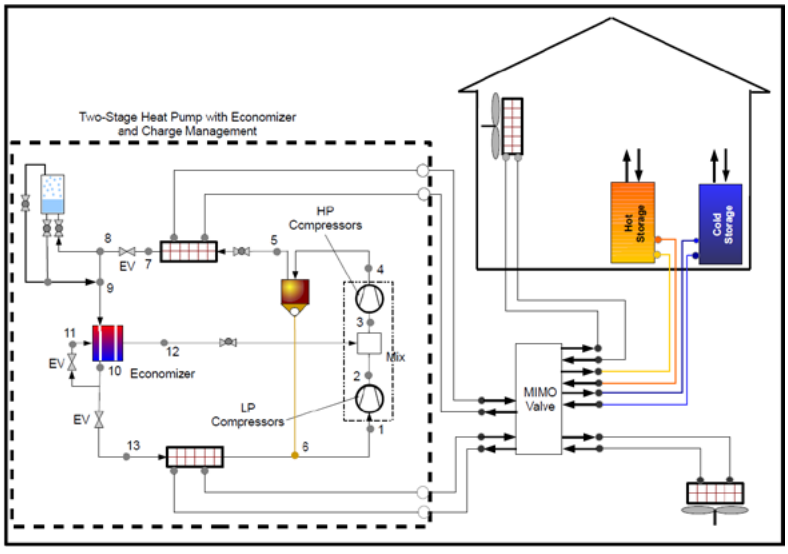

Fig. 2. Concept schematic of the packaged R-290 CCHP with secondary loops, external flow reversal, and possible coupling with cold and hot storage tanks.

The EG MIMO valve is used to direct flow into the home and has four sets of inputs and outputs. One set directs flow to an air-source heat exchanger exposed to the ambient to provide capacity modulation. The other three lead to the home, with one leading to an air-source heat exchanger to control the indoor environment and the other two leading to a hot and cold storage tank. This enables the system to utilize nearly 100% of the heat

pumped by the VCC, either at that moment or later on via thermal storage. This also enables grid-interaction with the system, as thermal storage can be used to eliminate the need to run the VCC during peak hours.

2.2. Seasonal weather and load calculations

The system design was based off of weather data from Typical Meteorological Year 3 (TMY3) [13], for the Boston Logan airport. This data contains, among other things, average dry bulb temperatures and relative humidity for every day in a typical year. This allowed the calculation of how many hours the heat pump system would need to run at the given operating conditions over the course of one year. Data from Boston is shown in **오류! 참조 원본을 찾을 수 없습니다.**. The design internal environment was 50% relative humidity with a dry bulb temperature of 21.1 ℃. Therefore, at 21.1 ℃ there was zero load, designating this temperature as the chosen balance point. A heat pump capacity of 5 tons was the design target, motivating a design capacity of 17.58 kW at -20 ℃. The target load profile is shown in Fig. 4. On the cooling side, a design temperature of 30 ℃ was chosen, and a sensible heat ratio (SHR) across the evaporator was assumed to be 0.7. This resulted in a design total cooling load of 7.3 kW after the consideration of occupants and other heat sources. It is assumed that each occupant creates 100 W of heat and that four occupants are in the home. Additionally, the lighting and appliance heat loads are assumed to be 750 W each. The complete cooling load calculation can be seen in Eqs. 1 through 5.

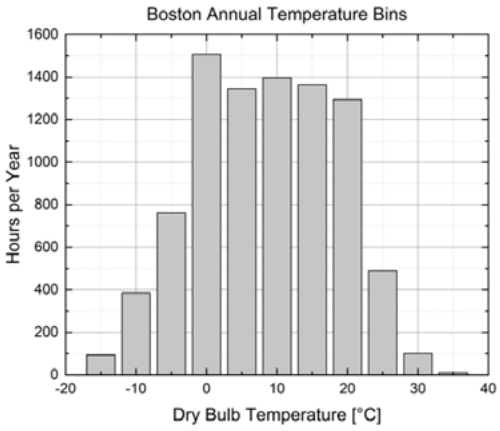

Fig. 3. Dry-bulb temperature bins for Boston over 1 year.

$$\dot{Q}_{\text{cool,sens}} = \frac{(T_{\text{amb,cooling}} - T_{\text{indoor}}) \cdot \dot{Q}_{\text{heat,design}}}{(T_{\text{indoor}} - T_{\text{amb,heat,design}})} \tag{1}$$

$$\dot{Q}_{\text{cool,sens}} = \dot{Q}_{\text{cool,base}} \cdot SHR \tag{2}$$

$$\dot{Q}_{\text{cool,base}} = \dot{Q}_{\text{cool,sens}} + \dot{Q}_{\text{cool,lat}} \tag{3}$$

$$\dot{Q}_{\text{int}} = \dot{Q}_{\text{occupant}} \cdot N_{\text{occupant}} + \dot{Q}_{\text{lighting}} + \dot{Q}_{\text{appliance}} \tag{4}$$

$$\dot{Q}_{\text{cool}} = \dot{Q}_{\text{cool,base}} + \dot{Q}_{\text{int}} \tag{5}$$

After these two capacities were specified along with the balance point, linearization was conducted for both heating and cooling mode to provide design capacities at individual ambient temperatures across the design range. These functions are shown in the load profile shown in Fig. 4.

When these loads are multiplied by the hours at which the heat pump needs to operate at these conditions (**오류! 참조 원본을 찾을 수 없습니다.**), the overall energy requirement for both heating and cooling can be calculated, in kWhr. These plots for heating are shown in Fig. 5, while cooling mode demand is shown in Fig. 6.

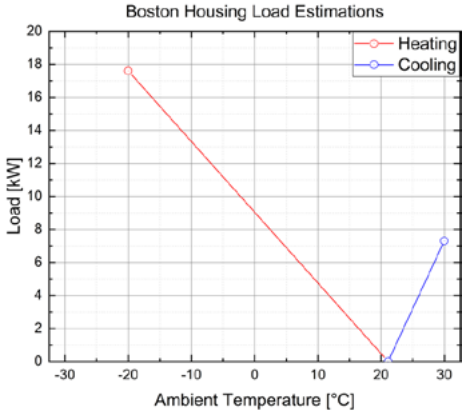

Fig. 4. Heat-pump design loads for Boston with balance point fixed at dry bulb temperature of 21.1 ℃ and 50% relative humidity.

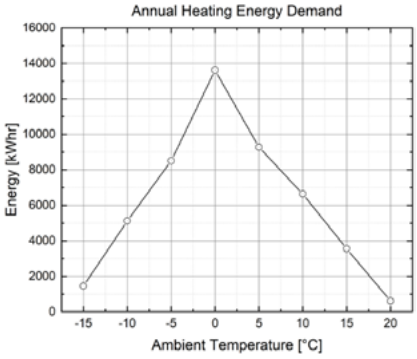

Fig. 5. Boston annual heating energy demand.

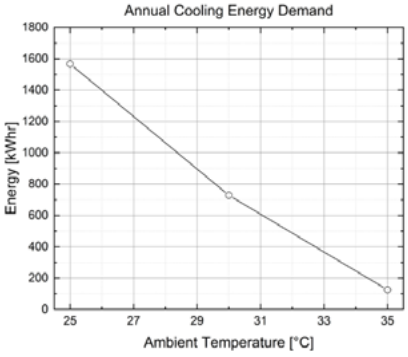

Fig. 6: Boston annual cooling energy demand.

2.3. Modeling overview

Once the loads are determined, a dynamic model was developed using the Modelica language [14] in a Dymola environment [15] utilizing the TIL Suite [16]. This form of modelling was chosen to enable both pseudo-steady state modelling, as will be conducted with the seasonal analysis herein, but also dynamic modelling for charge sensitivity and control strategy studies. The system within Dymola is shown in cooling mode in Fig. 7.

For a given operating condition, defined by the ambient temperature, indoor temperature, and required capacity, the primary method of performance quantification is the COP. The COP is the ratio of delivered capacity to power input, including only compressor power. The delivered capacity is defined as heat absorbed via the evaporator in cooling mode heat rejected via the condenser in heating mode and, shown in Eqs. 6 and 7, respectively.

$$COP_{\text{cool}} = \frac{\dot{Q}_{\text{evap}}}{\dot{W}_{\text{in}}} \tag{6}$$

$$COP_{\text{heat}} = \frac{\dot{Q}_{\text{cond}}}{\dot{W}_{\text{in}}} \tag{7}$$

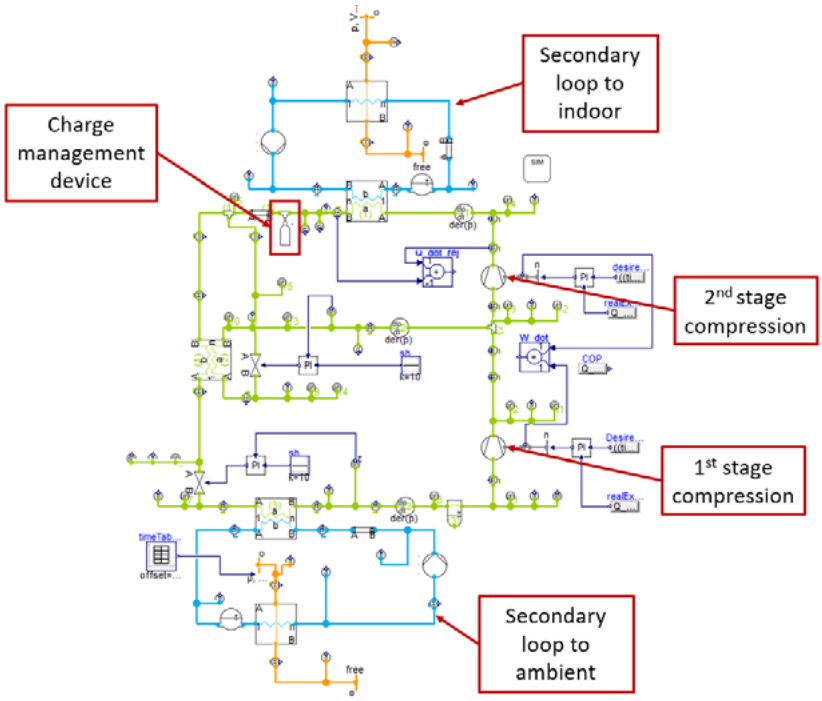

Fig. 7. View of the complete CCHP model within Dymola including secondary loops and charge management system.

Once the COP of the system is calculated it can be converted into two metrics that are more commonly used in industry for quantifying the performance of a system. These metrics are SEER and HSPF for cooling and heating modes, respectively. Both metrics are the ratio of desired heat transfer over the work input, which is the same as COP except for being seasonal averages. This means that each HSPF and SEER rating at an operating condition is weighted by how many hours the system operates at that condition, resulting in an assessment of seasonal performance. Additionally, COP takes both the numerator and denominator to have the same units, resulting in a dimensionless value. Both HSPF and SEER take the heating or cooling capacity in BTU, with the power input in Watt-hrs., resulting in a factor of 3.412 to convert from COP to the units for SEER and HSPF. The calculation of SEER and HSPF are shown in Eqs. 8 and 9.

$$SEER = \frac{\sum_{i=1}^{N} COP_i \cdot N_{\text{hours,i}}}{\text{Total Cooling Hours}} \tag{8}$$

$$HSPF = \frac{\sum_{i=1}^{N} COP_i \cdot N_{\text{hours,i}}}{\text{Total Heating Hours}} \tag{9}$$

The second shared component model is for the compressor, which follows a standard AHRI 10-Coefficient map that outputs mass flow rate as $\dot{m}_{\text{map}}$ and power consumption as $\dot{W}_{\text{in}}$ for a given condensation and evaporation temperature. The format for the map is shown in Eq. 10.

$$C_1 + C_2 \cdot T_{\text{evap}} + C_3 \cdot T_{\text{cond}} + C_4 \cdot T_{\text{evap}}^2 + C_5 \cdot T_{\text{evap}} \cdot T_{\text{cond}} + C_6 \cdot T_{\text{cond}}^2 + C_7 \cdot T_{\text{evap}}^3 + C_8 \cdot T_{\text{evap}}^2 \cdot T_{\text{cond}} + C_9 \cdot T_{\text{cond}}^2 \cdot T_{\text{evap}} + C_{10} \cdot T_{\text{cond}}^3 \quad (10)$$

The compressor is assumed to be variable speed, and the required speed is determined as a ratio of the mass flow rate given by the compressor map, $\dot{m}_{\text{map}}$, and the required flow rate across a given heat exchanger, $\dot{m}_{\text{Req'd}}$, determined from the simplified system model. As the authors were unable to obtain an experimental map for a variable speed R-290 compressor of this capacity, a map for a smaller variable speed R-290 scroll compressor was utilized and scaled up via speed as well as by the number of compressors in tandem for both the first and second stages to provide the desired capacity. This ratio is shown by Eq. 11, and the operation frequency is calculated by Eq. 12 for 60 Hz operation. The overall isentropic efficiency of the compressor is then calculated by Eq. 13.

$$Frac_{\text{speed}} = \frac{\dot{m}_{\text{req'd}}}{\dot{m}_{\text{map}}} \quad (11)$$

$$f_{60} = \text{Frac}_{\text{speed}} \cdot 60 \quad (12)$$

$$\eta_{\text{is,o}} = \frac{Frac_{\text{Speed}} \cdot \dot{m} \cdot (h_{2,\text{s}} - h_1)}{\dot{W}_{\text{in}}} \quad (13)$$

where

$$h_{2\text{s}} = f(p_2, s_1) \quad (14)$$

and

$$\dot{W}_{\text{in}} = Frac_{\text{Speed}} \cdot (h_2 - h_1) + \dot{Q}_{\text{comp}} \quad (15)$$

where

$$\dot{Q}_{\text{comp}} = 0.05 \cdot \dot{W}_{\text{in}} \quad (16)$$

Because the compressor map from Eq. 10 was calculated with a fixed suction superheat of 10 K, superheat correction was added to ensure an accurate prediction of compressor performance. Mass flow rate with a correction factor F of 0.75 and power consumption are corrected using Eqs. 17 and 18, respectively.

$$\frac{\dot{m}_{new}}{\dot{m}_{data}} = 1 + F \cdot \left(\frac{\rho_{suc,new}}{\rho_{suc,data}} - 1 \right) \quad (17)$$

$$\frac{\dot{W}_{new}}{\dot{W}_{data}} = \frac{\dot{m}_{new}}{\dot{m}_{data}} \cdot \frac{\Delta h_{s,new}}{\Delta h_{s,data}} \quad (18)$$

Table 1. Heat exchanger pressure drop and heat transfer correlations.

Heat Exchanger	Heat Transfer	Pressure Drop
Fin-and-Tube, R-290 Side	Gnielinski [18]; Dittus, and Boelter [19]	Konakov for Smooth Pipes [20]
Fin-and-Tube, Air Side	Haaf [21], constant η [22] (Assumed to be 0.9)	Haaf [21]
Plate IHX	Evaporation: Shah [23] Chen [24] / Condensation: Shah [25] / 1-Phase: Gnielinski [18], Dittus, and Boelter [19]	Konakov for Smooth Pipes [20]
Plate HX, R-290 Side	Evaporation: Longo [26] Condensation: Longo [27]/ Gnielinski, Dittus, and Boelter	Quadratic Mass Flow Dependent [28]
Plate HX, EG Side	VDI Plate Alpha [29]	VDI Single-Phase [29]

This CCHP utilizes two types of heat exchangers, and both models assumed homoegenous equilibrium flow. The EG to air are fin-and-tube heat exchangers, while the R-290 to EG transfer utilizes plate heat exchangers.

The dimension of these heat exchangers were obtained through a separate modeling effort using a tool from Bell et al. [17] known as ACHP. Additionally, to conservatively estimate secondary loop losses, an extra 20% load was placed on the R-290 side of the cycle. A summary of heat transfer and pressure drop correlations utilized is provided in Table 1.

3. Results and Discussion

A full piping and instrumentation diagram (P&ID) is provided in Fig. 8 to offer a detailed schematic of the VCC aspect of this work. To simulate the TMY3 data, both ambient temperature and the required capacity for that temperature needed to be actively called into the model. This was completed by utilizing an externally-defined table that drove conditions assessed in the model. Fig. 9 shows the ability of the model to import TMY data as an air-temperature inlet value over the course of a year, and Fig. 10 shows the P-h diagram ability of the model, following the nomenclature from Fig. 8. Capacity modulation is to be achieved through control of the compressor speeds along with active modulation of the EXVs via proportional-integral (PI) control.

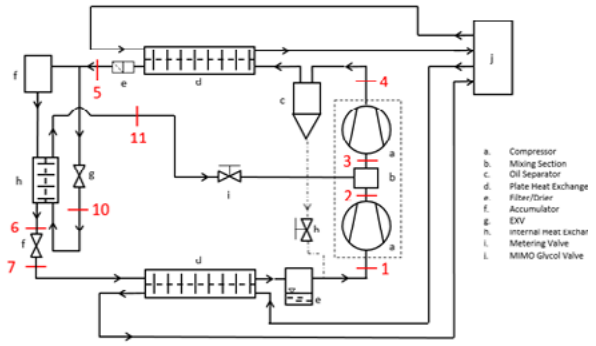

Fig. 8. P&ID of the proposed VCC.

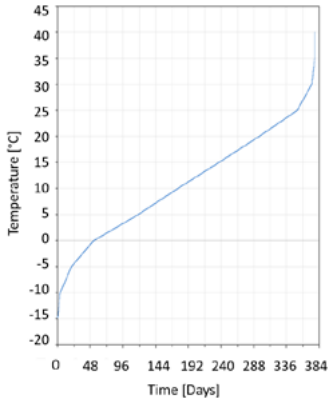

Fig. 9. 1 Year of TMY data for Boston in Dymola.

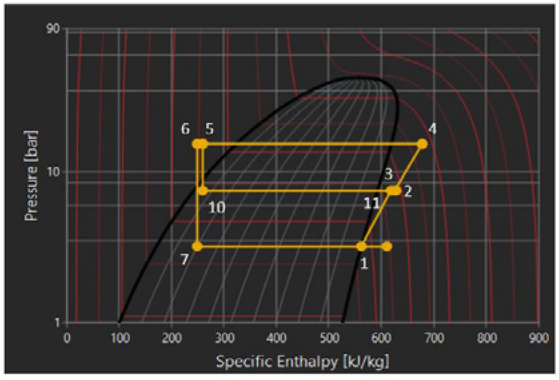

Fig. 10. P-h diagram of R-290 system in Dymola.

Preliminary results were achieved with a steady-state model of similar fidelity, which are presented in this section. These results include supplementary electrical heating to achieve the desired heating capacity. To identify the amount of supplementary capacity, the sources of heating capacity is differentiated between compressors and supplementary electric heating in Fig. 11. COP calculation with supplementary resistive heating is calculated using Eq. 19, where the COP of the electric heating is assumed to be the ideal value of 1.

$$COP_{\text{weighted}} = \frac{COP_{\text{VCC}} \cdot \dot{Q}_{\text{VCC}} + (1) \cdot \dot{Q}_{\text{elec}}}{\dot{Q}_{\text{total}}} \quad (19)$$

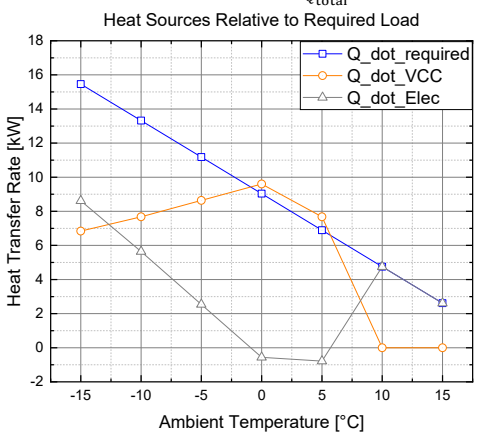

Fig. 11. Heat source variation with ambient temperature and associated load.

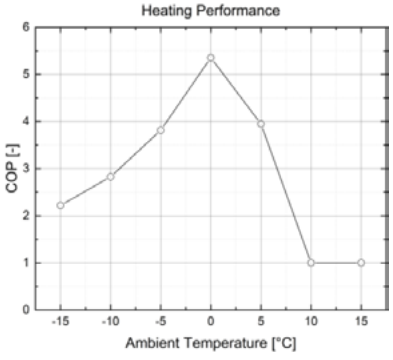

Fig. 12. Seasonal COP in heating mode.

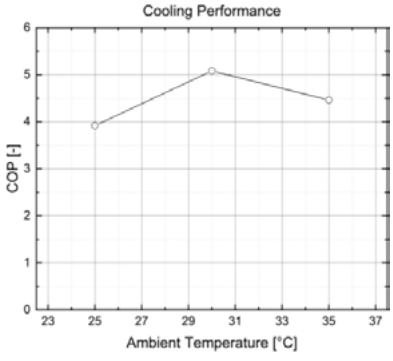

Fig. 13. Seasonal COP in cooling mode.

Tandem compressors were utilized, and variable speed inputs were used to simulate engaging and disengaging compressors to provide as much capacity as possible. This system achieved a SEER rating of 14.1 and an HSPF of 10.1. Seasonal COP results from the model are provided for heating and cooling modes in Fig. 12 and Fig. 13, respectively.

Being R-290 an A3 refrigerant, charge minimization while guaranteeing system performance throughout the season is a very important aspect to be investigated. The dynamic model was utilized to simulate performance of the system in heating mode, including dependence of the charge of the system. This was accomplished through a parametric study which used time dependent ambient and heating load conditions across a range of imposed system charges. The charge modulation has been accomplished by including a charge filling station on liquid line after the condenser, as shown in Fig.7. These conditions are embodied in Fig. 14 for the ambient condition in dependence of time during the dynamic simulation.

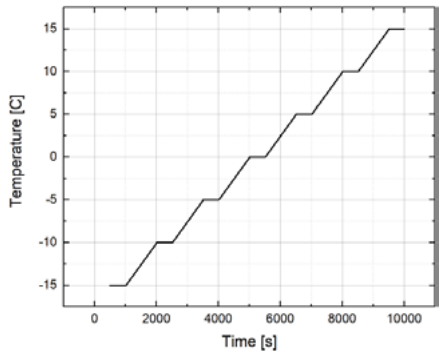

Fig. 14 Simulated heating season across a range of -15 ℃ to 15 ℃

The periods of steady temperature are taken from Fig. 4 in increments of 5 ℃. These were simulated across a range from -15 ℃ to 15 ℃ via a time dependent table interpolation. A curve fit of the heating load data from Fig. 4 allowed the calculation of the heating load at each point in time according to the ambient temperature. Finally, a total charge was imposed upon the system across each simulated heating season to find an optimal minimal charge that ensures system performance across the heating season while minimizing hazards of excessive charge inside the system. This study was conducted across a range of system charge from 0.1 kg to 0.6 kg.

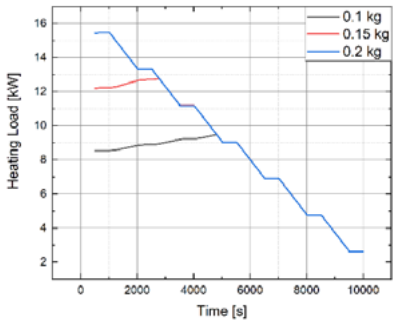

Fig. 15 Simulated heating performance in dependence of total system charge

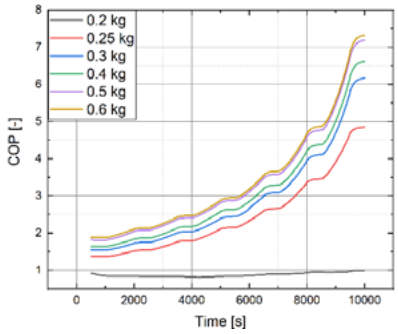

Fig. 16 Simulated heating COP in dependence of total system charge

The first criteria for the minimum charge required was to achieve the heating load determined by the ambient condition. As seen in **오류! 참조 원본을 찾을 수 없습니다.**, the system began to meet the heating demand at a system charge of 0.2 kg. This was taken as an absolute minimum charge, but the system COP, as shown in **오류! 참조 원본을 찾을 수 없습니다.**, indicated poor system performance at this charge amount. As expected, the system COP increased with increasing charge until diminishing returns were observed at higher amounts of system charge, serving as a maximum realistic amount of charge within the system. A system charge between 0.4 kg and 0.5 kg is clearly indicated as the optimal charge in the system, as an increase to 0.6 kg provided little benefit in system performance.

4. Conclusions and Recommendations

A multi-stage VI CCHP architecture using R-290 as the refrigerant has been proposed and was coupled to a novel EG secondary loop connected to a residential home. The target environment is the northern US, so TMY3 data from Boston, USA was utilized, and dry bulb temperature bins were developed for one year. A target heating capacity of 5 tons (17.58 kW) at -20 ℃ was chosen with a suggested balance point of 21.1 ℃

and 50% relative humidity indoor condition to provide a seasonal load profile. A dynamic modeling structure was developed and described, and the TMY temperatures were input. However, COP calculations using seasonal loads and temperatures were performed using a steady-state model with similar assumptions. These calculations were then used to provide both seasonal performance calculations for the proposed architecture as well as a reference parameters and results for further dynamic modeling development. The proposed cycle was able to achieve a SEER value of 14.1 and an HSPF of 10.1. Finally, charge minimization was performed with respect to system performance in terms of heating load demand and system COP to ensure both the performance and safety of the system to be constructed. A preliminary charge estimation of 0.45 kg to meet heating demand and moderate system COP was calculated. Future work is to repeat the seasonal calculations with the proposed dynamic model and further assess control algorithms and active charge management to leverage the dynamic modeling abilities. Furthermore, a potential prototype system is being developed for experimental validation.

5. Acknowledgements

The authors would like to thank IMBY Energy for financial support and the faculty and staff of the Ray W. Herrick Laboratories for technical and financial support.

Nomenclature

C	Compressor map coefficient	-
E	Energy	kWhr
F	Frequency	Hz
Frac	Fraction	-
h	Specific enthalpy	kJ/kg
m	Mass	kg
$\dot{m}$	Mass flow rate	kg/s
N	Number	-
$\dot{Q}$	Heat transfer rate	kW
T	Temperature	℃
$\dot{W}$	Power	kW

Greek Symbols

η	Efficiency	-
Δ	Change	-
ρ	Density	kg/m^3

Subscript

amb	Ambient
base	Base load
comp	Compressor
cond	Condenser
cool	Cooling
data	Data
elec	Electric
evap	Evaporator
heat	Heating
i	Index
in	Inlet
int	Internal
is,o	Overall isentropic
lat	Latent
map	Map
new	New
s	Isentropic
sens	Sensible

Acronyms

CCHP	Cold-Climate Heat Pump
COP	Coefficient of Performance
EG	Ethylene-Glycol
ELLA	Electronic Liquid Level Actuator
EXV	Electronic Expansion Valve
GWP	Global Warming Potential
HFC	Hydrofluorocarbon
HP	High Pressure
HSPF	Heating Seasonal Performance Factor
HX	Heat Exchanger
IHX	Internal Heat Exchanger
MIMO	LP
MIMO	Multi-Input Multi-Output
ODP	Ozone Depletion Potential
PAG	Polyalkylene Glycol
PHX	Plate Heat Exchanger
PI	Proportional Integral
POE	Polyolester
P&ID	Piping and Instrumentation Diagram
SEER	Seasonal Energy Efficiency Ratio
SHR	Sensible Heat Ratio
TMY3	Typical Meteorological Year
VCC	Vapor-Compression Cycle
VI	Vapor Injected

References

[1] NEEP, "Northeast / Mid-Atlantic Air-Source Heat Pump Market Strategies Report," 2014.

[2] USDOE and EERE, "Minimum Efficiency Requirements for Air-Source and Geothermal Heat Pumps," 2019.

[3] K. Wang, M. Eisele, Y. Hwang, and R. Radermacher, "Review of secondary loop refrigeration systems," *Int. J. Refrig.*, vol. 33, no. 2, pp. 212–234, 2017.

[4] B. Palm, "Hydrocarbons as refrigerants in small heat pump and refrigeration systems – A review," vol. 31, pp. 552–563, 2008.

[5] K. Park and D. Jung, "Thermodynamic performance of HCFC22 alternative refrigerants for residential air-conditioning applications," vol. 39, pp. 675–680, 2007.

[6] P. Fernando, B. Palm, P. Lundqvist, and E. Granryd, "Propane heat pump with low refrigerant charge : design and laboratory tests," vol. 27, pp. 761–773, 2004.

[7] P. Ginies, P. Dewitte, M. F. Terrier, and M. Charni, "Low GWP Refrigerant and Partial Miscible Lubricant," *Proc. 23rd Int. Compress. Eng. Conf. Purdue*, p. Paper 2700, 2014.

[8] X. Xu, Y. Hwang, and R. Radermacher, "Transient and steady-state experimental investigation of flash tank vapor injection heat pump cycle control strategy," *Int. J. Refrig.*, vol. 34, no. 8, pp. 1922–1933, Dec. 2011.

[9] S. S. Bertsch and E. A. Groll, "Two-stage air-source heat pump for residential heating and cooling applications in northern U.S. climates," *Int. J. Refrig.*, vol. 31, no. 7, pp. 1282–1292, Nov. 2008.

[10] M. M. Mathison, J. E. Braun, and E. A. Groll, "Performance limit for economized cycles with continuous refrigerant injection," *Int. J. Refrig.*, vol. 34, no. 1, pp. 234–242, 2010.

[11] S. L. Caskey and D. Kultgen, "Simulation of an Air-Source Heat Pump with Two- Stage Compression and Economizing for Cold Climates," 2012.

[12] A. Gschwend, T. Menzi, S. Caskey, E. A. Groll, and S. S. Bertsch, "Energy consumption of cold climate heat pumps in different climates – Comparison of single-stage and two-stage systems," *Int. J. Refrig.*, vol. 62, pp. 193–206, 2016.

[13] NREL, "Typical Meteorological Year Data (TMY)," *1991-2005 Update*, 2019. [Online]. Available: https://rredc.nrel.gov/solar/old_data/nsrdb/1991-2005/tmy3/.

[14] S. E. Mattson, H. Elmqvist, and J. F. Broenink, "Modelica: An international effort to design the next generation modelling language," *J. A, Benelux Q. J. Autom. Control*, vol. 38, no. 3, pp. 16–19, 1998.

[15] "Dassault Systems - DYMOLA Systems Engineering," 2019.

[16] TLK-thermo, "TIL Suite simulates Thermal Systems." 2018.

[17] I. H. Bell, "Air conditioning and heat pump mpdel (ACHP) source code version 1.5." p. Online; accessed 10-Sept-2019, 2015.

[18] V. Gnielinski, "New equations for heat and mass transfer in turbulent pipe and channel flow," *Int. Chem. Eng.*, vol. 16, no. 2, pp. 359–368, 1976.

[19] H. D. Baehr and K. Stephan, *Waerme-und Stoffuebertragung, 2 Auflage*. Springer, 1996.

[20] P. K. Konakov, "A new correlation for the friction coefficient in smooth tubes," *Berichte der Akad. der Wissenschaften der UDSSR*, vol. 51, p. 51, 1946.

[21] S. Steimle, *Handbuch der Kaeltetechnik, Waermeuebertragung in Luftkuehlern*. Springer, 1988.

[22] Schmidt, "Heat transfer calculations for extended surfaces," *Refrig. Eng.*, vol. 57, pp. 251–357, 1949.

[23] M. M. Shah, "A new correlation for heat transfer during boiling flow through pipes," *ASHRAE Trans.*, vol. 82, pp. 66–86, 1976.

[24] J. C. Chen, "A correlation for boiling heat transfer to saturated fluids in convective flow," *Ind. Eng. Chem. Process Des. Dev.*, vol. 5, no. 3, pp. 322–329, 1966.

[25] M. M. Shah, "A general correlation for heat transfer during film condensation inside pipes," *Int. J. Heat Mass Transf.*, vol. 22, no. 4, pp. 547–556, 1979.

[26] G. A. Longo, S. Mancin, G. Righetti, and C. Zilio, "International Journal of Heat and Mass Transfer A new model for refrigerant boiling inside Brazed Plate Heat Exchangers (BPHEs)," *Int. J. Heat Mass Transf.*, vol. 91, pp. 144–149, 2015.

[27] G. A. Longo, G. Righetti, and C. Zilio, "International Journal of Heat and Mass Transfer A new computational procedure for refrigerant condensation inside herringbone-type Brazed Plate Heat Exchangers," *Int. J. Heat Mass Transf.*, vol. 82, pp. 530–536, 2015.

[28] W. Wagner, *Stroemung und Druckverlust*. Vogel, 2008.

[29] H. Martin and T. Kit, "VDI Heat Atlas," *VDI Heat Atlas*, 2010.